Solvation of Li^+ by Acetone, THF, and Diethyl Ether in the Gas Phase and the Ion−Molecule Association Mechanism

Russell L. Jarek,[†,‡] Terrence D. Miles,[†,§] Michelle L. Trester,[†,∥] Stephen C. Denson,[†,⊥] and Seung Koo Shin*[,†,#]

Department of Chemistry, University of California, Santa Barbara, California 93106, and Department of Chemistry, Pohang University of Science and Technology, San 31 Hyoja-dong Namgu, Pohang, Kyoungbuk, Korea 790-784

Received: March 3, 1999; In Final Form: July 8, 1999

Fourier transform ion cyclotron resonance spectrometry has been employed to study the solvation of the Li^+ ion with acetone, tetrahydrofuran (THF), and diethyl ether (DEE) in the gas phase. $LiILi^+$ triple ions are produced in the ICR cell by the laser desorption ionization of a lithium iodide/dibenzo-18-crown-6-ether matrix pasted on a Teflon substrate. All O donors abstract Li^+ from the triple ion and form solvated complexes with a maximum solvation number of three at room temperature, around 10^{-6} Torr. All third solvent binding energies are determined from van't Hoff plots. Structures and energetics of the $Li^+\cdot(S)_n$ complexes, where $n = 1-4$ for acetone and THF and $n = 1-3$ for DEE, have been calculated at the Hartree−Fock level with a 6-311+G(d,p) basis set. Solvation enthalpies and free energies are calculated, and solvent binding enthalpies are compared with experiments. The kinetics of solvent exchange and the association reactions of $Li^+\cdot$(acetone-h_6)(acetone-d_6) with a 1:1 acetone-h_6/acetone-d_6 mixture have been measured as a function of pressure. The lifetime of the collision complexes are derived and compared with phase space theory calculations. The isotope effect on the radiative cooling rate is discussed.

Introduction

The lithium cation is remarkable for its ready formation of solvated complexes and ion aggregates,[1] thereby affecting the chemical reactions and ion conductivities of lithium electrolytes in condensed phase, either directly or through its "salt effect."[2,3] Noncovalent interactions between Li^+ and electron donors are the driving force behind the formation of solvated complexes, whereas ionic interactions between Li^+ and the counterions influence the extent of solvation and ion association. Each of these interactions are of fundamental importance to molecular recognition and the mobility of the lithium ion in condensed phase. A detailed understanding of these interactions can be achieved through quantitative studies of the solvation energetics in the gas phase, in which the solvated $Li^+\cdot(\text{molecule})_n$ clusters can be formed, isolated, and allowed to reach thermal equilibria with gaseous solvents. In the present study, we examine simple $Li^+\cdot(\text{solvent})_3$ systems in which the solvents are acetone, tetrahydrofuran, and diethyl ether.

Direct gas-phase studies of the thermodynamic properties of Li^+−solvent interactions began three decades ago with Dzidic and Kebarle using high-pressure mass spectrometry.[4] They determined the absolute bond enthalpies and entropies of alkali-metal ions with one to six water molecules. The values for Li^+-H_2O were not measured directly because of experimental difficulties. Instead, they were extrapolated from the values determined for larger $Li^+-(H_2O)_{2-6}$ clusters. Since then, reactions of Li^+ with π- and n-donor bases were studied by Wieting et al.[5] using ion cyclotron resonance (ICR) spectrometry, and their binding energies relative to the Li^+-OH_2 bond energy, estimated by Dzidic and Kebarle,[4] were reported by Beauchamp and co-workers.[6−8] Recently, Taft et al.[9] reported the free energy of formation of $Li^+\cdot$(molecule) adducts for 110 organic bases at 373 K, referenced to the free energy of formation for $Li^+\cdot(NH_3)$ reported by Woodin and Beauchamp.[7] From direct comparisons of their free energies, Taft et al. found an interesting correlation of basicities toward H^+ and Li^+.[9] To settle the Li^+ affinity scale on a more firm base, Rodgers and Armentrout measured the Li^+-OH_2 bond energies in $Li^+(H_2O)_n$, $n = 1-6$, by collision-induced dissociation (CID), and recommended a reference value of $D_{298}(Li^+-OH_2) = 32.7$ kcal mol^{-1} for $Li^+(H_2O)$.[10] In addition, Armentrout and co-workers determined bond energies of the lithium cation with dimethyl ether (DME),[11] 1,2-dimethoxyethane and 12-crown-4-ether,[12] and a series of short-chain alcohols.[13,14] Today, with rapid advances in molecular recognition and the development of lithium batteries, there are critical needs for the thermodynamic solvation data of Li^+ in various organic solvents.

During our studies of solvations of $LiXLi^+$ (X = halide) triple ions in the gas phase,[15,16] we found a means to produce thermalized and solvated lithium cations in the ICR cell. The $LiILi^+$ triple ion generated by matrix-assisted laser desorption ionization (MALDI)[17−19] underwent Li^+-abstraction reactions with O-donor solvents in competition with, or preferential to, associative solvation. Further solvation of the $Li^+\cdot S$ complex, *S* being a solvent molecule, occurred spontaneously, on the time scale of 1 s, until the solvation equilibrium was attained.

* E-mail: skshin@postech.ac.kr. Fax: +82-562-279-3399.
† University of California−Santa Barbara
Present address: Sandia National Laboratories, P.O. Box 5800, Albuquerque, NM 87185-1407.
Present address: Citrus College, 1000 West Foothill Boulevard, Glendora, CA 91741-1899
∥ Present address: The Rockefeller University, 1230 York Ave, New York, NY 10021.
⊥ Present address: Department of Chemistry, University of Arizona, Tucson, AZ 85721.
Pohang University of Science and Technology

10.1021/jp9908193 CCC: $19.00
Published on Web 02/23/2000

Utilizing this abstraction method to generate solvated lithium ions has considerable merit: First, unlike a thermionic source, MALDI does not warm the ICR cell, thereby affording an accurate temperature reading. Second, this first solvation, via abstraction, occurs several orders of magnitude faster than would the associative solvation, via radiative relaxation and collisional quenching, under the low-pressure ICR conditions ($\sim 1 \times 10^{-6}$ Torr or less). Last, the direct solvation equilibrium measurement leads to absolute bond enthalpies, whereas other ICR solvent-exchange equilibrium measurements yield relative free energies. When compared with CID threshold measurements, our ICR equilibrium methodology is free from kinetic shift, thanks to ion trapping. Although CID is a direct measurement, the CID data analysis has to deal with a large kinetic shift in highly solvated systems, making the final results dependent on the modeling of the transition state and the collisional energy transfer processes.[14,20] As with all methods, there are some limitations to the direct equilibrium measurements performed in the Fourier transform ion cyclotron resonance (FT-ICR) environment. The pressure range available is lower bound by the need to limit the reaction time to obtain equilibrium (low 10^{-7} Torr) and upper bound by collisional damping of the transient detection signal (mid-10^{-6} Torr). In addition, there is currently a narrow temperature range utilized on the system, 15−90 °C, which limits thermodynamic determinations of the bond dissociation enthalpy (BDE) to the 15−25 kcal mol^{-1} range.

In this work, the BDEs were determined for $Li^+ \cdot (S)_3$ complexes with acetone, tetrahydrofuran (THF), and diethyl ether (DEE). To obtain information about the lifetime of bimolecular ion−molecule collision complexes, the kinetics of dissociative solvent exchange and associative solvation were measured as a function of pressure for the lithium−acetone system. In addition, theoretical calculations were carried out for all of the $Li^+ \cdot S_n$ complexes observed and experimental BDEs are compared with the theory. In light of theoretical energetics and equilibrium structures, the steric effects on solvation are elucidated. Theoretical molecular parameters and energetics also permit phase space theory (PST) calculations[21−23] of the lifetimes of collision complexes for direct comparisons with the experiments.

Experimental Section

Experimental setups were previously described in detail.[24] Experimental procedures pertinent to the present study are outlined below. The FT-ICR spectrometer used in this study consisted of a 1.2 T electromagnet (Varian), a vacuum chamber with a 1.85 in. cubic trapping ICR cell, and an FT-data system (IonSpec Inc., Omega/386) for data acquisition. There were 0.325-in. holes in the centers of the receiver plates, for optical access. A $^3/_8$-in. diameter Teflon substrate was mounted on a copper plug close to, but outside of, the ICR cell, near the center of the receiver plate. The ions that were trapped within the ICR cell and the neutral molecules flowing into the cell were able to reach thermal equilibrium in the 15−90 °C temperature range by warming both the vacuum chamber and the sample-inlet line with heating pads or by cooling them with air. The temperature of the chamber was measured at two different regions with type-K thermocouples in contact with the chamber but insulated from the ambient air.

A mixture of lithium iodide salt/dibenzo-18-crown-6-ether was dissolved in a 1:1 water/acetonitrile solution with methanol added to mix the aqueous and organic layers. The mixture was loaded on a Teflon substrate and then vacuum-dried to a visible layer. The 308-nm output from a XeCl excimer laser (Lambda-Physik, EMG-53 MSC) was used for the desorption ionization, with a typical pulse width of ~10 ns. The laser beam was mildly focused to ~2 mm diameter to desorb lithium salt ions. A typical laser power used in the desorption−ionization was ~2 mJ.

The background pressure in the ICR chamber was typically below 6×10^{-8} Torr. Gaseous samples entered into the ICR chamber through a Varian leak valve. The sample pressures were measured by calibrating the ion-gauge mounted in the ICR chamber against a capacitance manometer (MKS Baratron head 390HA-00010). The pressure extrapolation, less than 2 orders of magnitude, is estimated to have an accuracy of ±25%. For the rate constant measurements, ion signals were monitored as a function of time delay, and the results were simulated with pseudo-first-order reaction kinetics by a least-squares fitting program.

All of the chemicals were purchased from Aldrich, Inc., and were used after several freeze−pump−thaw cycles. The purity of each sample was tested by examination of their EI mass spectra. Sample-inlet lines were baked and pumped out overnight to prevent any cross-contamination between samples.

All calculations were performed by use of the Gaussian-94 suite of programs[25] on a Silicon Graphics Power Indigo2 workstation and on a Digital Alpha 500AU power workstation. Geometries of the complexes of Li^+ with acetone, THF, and DEE were optimized at the HF level with a standard 6-311+G-(d,p) basis set.[26] The vibrational frequencies were calculated at the HF/6-31G* level. The solvent binding energies were corrected for zero-point energies that were scaled by 0.9135.[27] The solvation enthalpies and free energies were calculated using statistical mechanics.

Results

The BDEs of $Li^+ \cdot (S)_n$ complexes can be determined from the gas-phase equilibrium eq 1

$$Li^+ \cdot (S)_{n-1} + S \rightleftarrows Li^+ \cdot (S)_n \tag{1}$$

where S represents the solvent. The initial ion solvation was accomplished by the abstraction of Li^+ by O-donor solvents from the $LiILi^+$ triple ion with the rate constant of 2.2×10^{-9} cm^3 $molecule^{-1}$ s^{-1}. In contrast, the rate constant for the direct association of acetone to the bare Li^+ ion was reported to be $0.2-0.3 \times 10^{-9}$ cm^3 $molecule^{-1}$ s^{-1} in the $0.1-1.0 \times 10^{-6}$ Torr pressure range.[8] Further solvation occurred spontaneously on the order of tenths of seconds, with the final equilibrium being reached within 10−15 s at the experimental pressures used. Once the equilibrium constant is determined as a function of temperature, the thermochemical values can be derived from eqs 2 and 3.

$$\ln K_{eq} = -\frac{\Delta H}{RT} + \frac{\Delta S}{R} \tag{2}$$

$$K_{eq} = \frac{[Li^+ \cdot (S)_n]}{[Li^+ \cdot (S)_{n-1}] \cdot \left[\dfrac{P(S)}{P^o(1\ \text{atm})}\right]} \tag{3}$$

where K_{eq} is the standard state equilibrium constant determined from measured ion intensities, ΔH and ΔS are the enthalpy and the entropy of solvation, respectively, R is the gas constant, T is the temperature, and $P(S)$ is the partial pressure of the solvent. The fact that equilibrium had been truly obtained was checked

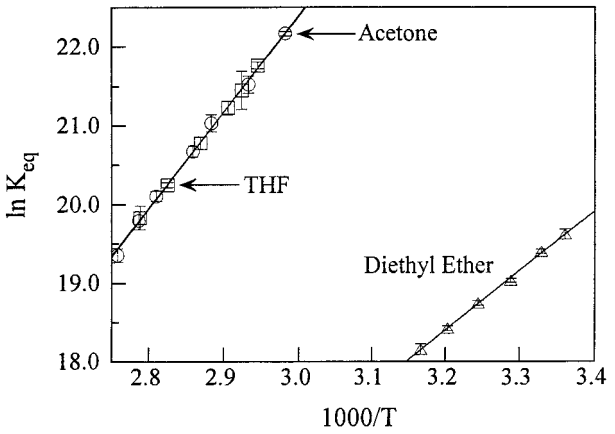

Figure 1. van't Hoff plots for the reaction 1. K_{eq} was determined by eq 3 and $n = 3$ for all three solvents: acetone (○), THF (□), and DEE (△). Error bars represent the standard deviation of ln K_{eq} taken from at least six measurements at each temperature.

TABLE 1: Optimized Parameters and Bond Dissociation Energies for $(S)_{n-1}\cdot Li^+$-*S* from RHF/6-311+G(d,p) Calculations

species	symm	Li···O (Å)	C−O (Å)	∠CXC[a] (deg)	D_0 (kcal mol^{-1})
acetone	C_{2v}		1.188	116.6	
Li^+·acetone	C_2	1.746	1.216	118.4	48.2
Li^+·(acetone)$_2$	D_2	1.792	1.210	118.1	37.7
Li^+·(acetone)$_3$	D_3	1.858	1.203	117.7	23.0
Li^+·(acetone)$_4$	S_4	1.954	1.201	117.5	12.7
THF	C_1		1.409	111.3	
Li^+·THF	C_1	1.798	1.451	110.5	43.9
Li^+·(THF)$_2$	C_2	1.840	1.443	110.7	35.5
Li^+·(THF)$_3$	C_3	1.898	1.435	110.8	23.3
Li^+·(THF)$_4$	S_4	1.976	1.428	110.8	14.1
DEE	C_{2v}		1.396	114.8	
Li^+·DEE	C_{2v}	1.807	1.430	115.2	42.9
Li^+·(DEE)$_2$	D_{2d}	1.861	1.426	114.1	32.5
Li^+·(DEE)$_3$*b*	C_2	1.959/1.940	1.422/1.425	112.7/114.9	13.6

[a] ∠CCC for acetone species, ∠COC for others. [b] Geometric parameters for this species are the one trans DEE and the two trans-gauche DEEs, respectively.

by the ejection of the $Li^+\cdot(S)_{n-1}$ species and by the observation of its return to the equilibrium proportion.

Bond Dissociation Enthalpies for $(S)_2\cdot Li^+-S$. The ratios of solvated ions were measured as a function of temperature. The resulting van't Hoff plots are shown in Figure 1. Because of limitations on the temperature range, only the $n = 3$ solvation enthalpies could be determined. Acetone and THF were examined at the high-temperature range (up to 90 °C), whereas DEE was studied in the low-temperature range (down to 15 °C). The bond dissociation enthalpies for acetone, THF, and DEE were measured to be -24.4 ± 0.6, -24.1 ± 0.6, and -15.0 ± 0.4 kcal mol^{-1}, respectively. Errors represent a 95% confidence interval as derived from the van't Hoff slopes.

Structures and Energetics of $Li^+\cdot(S)_n$ Complexes. Geometries were optimized at the restricted Hartree−Fock (RHF) level for $Li^+\cdot(S)_n$ complexes up to a maximum solvation number of $n = 4$ for acetone and THF and $n = 3$ for DEE with a 6-311+G(d,p) basis set. Selected optimized parameters and BDEs are listed in Table 1. In general, the oxygen nonbonding electrons form a dative bond with the lithium cation by pointing the O end of the solvent dipole toward Li^+. The Li−O coordination is linear in $Li^+\cdot(S)_2$, trigonal in $Li^+\cdot(S)_3$, and tetrahedral in $Li^+\cdot(S)_4$. As the solvation number increases, the Li−O bond distances increase, and the bond dissociation energies decrease.

The structures for $Li^+\cdot(acetone)_{2-4}$ are shown in Figure 2.

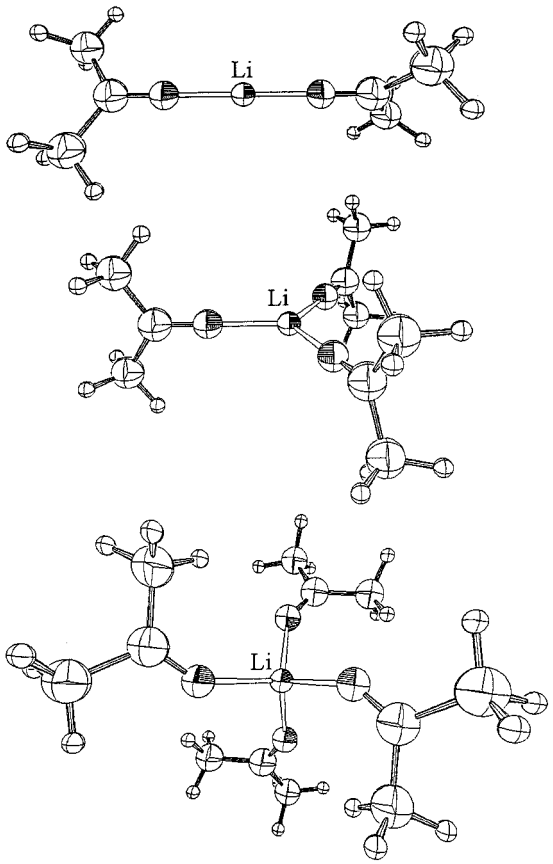

Figure 2. Calculated HF/6-311+G(d,p) structures for $Li^+\cdot(acetone)_{2-4}$. Oxygen atoms are partially shaded. The energetics and some geometrical parameters for all three structures are given in Table 1.

The coordination of acetone to Li^+ results in the loss of a plane of symmetry from free-C_{2v} acetone as the methyl groups counter-rotate. The C−O−Li angle is linear for $n = 1-3$, whereas it is bent to 148° in $n = 4$, which is suggestive of steric hindrance among the methyl groups. In going from $n = 1$ to $n = 4$, the Li−O bond distance gradually increases from 1.746 to 1.954 Å in increments of 0.046, 0.066, and 0.096 Å, respectively, whereas the C−O bond distance decreases from 1.216 to 1.201 Å by decrements of 0.006, 0.007, and 0.002 Å, respectively. As the C−O bond decreases, the C−C−C bond angle decreases concomitantly. In free acetone, the optimized C−O bond distance is 1.188 Å, and the C−C−C bond angle is 116.6°. The calculated Li^+−acetone bond energies are 48.2, 37.7, 23.0, and 12.7 kcal mol^{-1} for $n = 1-4$, respectively. The total solvation energy for $Li^+\cdot(acetone)_4$ is 121.6 kcal mol^{-1}.

The structures for $Li^+\cdot(THF)_{2-4}$ are shown in Figure 3. Unlike $Li^+\cdot(acetone)_4$, there is no distortion in the planar Li−O−$(C)_2$ geometry for any of the $n = 1-4$ complexes. In going from $n = 1$ to $n = 4$, the Li−O bond distance gradually increases from 1.798 to 1.976 Å in increments of 0.042, 0.058, and 0.078 Å, whereas the C−O bond distance decreases from 1.451 to 1.428 Å by decrements of 0.008, 0.008, and 0.007 Å. As the C−O bond decreases, the C−O−C bond angle increases concomitantly. In free THF, the optimized C−O bond distance is 1.409 Å, and the C−O−C bond angle is 111.3°. The calculated Li^+−THF bond energies are 43.9, 35.5, 23.3, and 14.1 kcal mol^{-1} for $n = 1-4$, respectively. The total solvation energy for $Li^+\cdot(THF)_4$ is 116.8 kcal mol^{-1}.

The structures for $Li^+\cdot(DEE)_{1-3}$ are shown in Figure 4. All of the ethyl groups in $Li^+\cdot(DEE)_{1-3}$ are in the staggered conformation. Structures for $Li^+\cdot(DEE)_{1-2}$ are very similar to

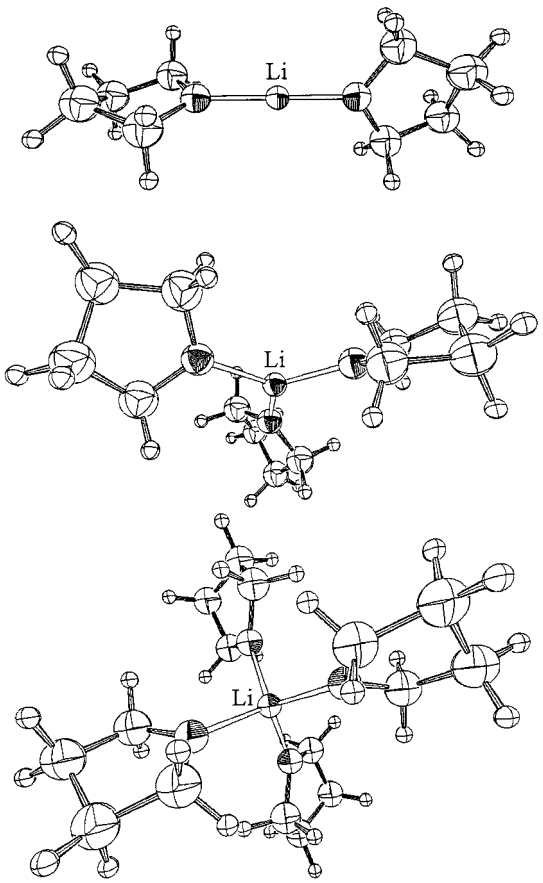

Figure 3. Calculated HF/6-311+G(d,p) structures for $Li^+\cdot(THF)_{2-4}$. Oxygen atoms are partially shaded. The energetics and some geometrical parameters for all three structures are given in Table 1.

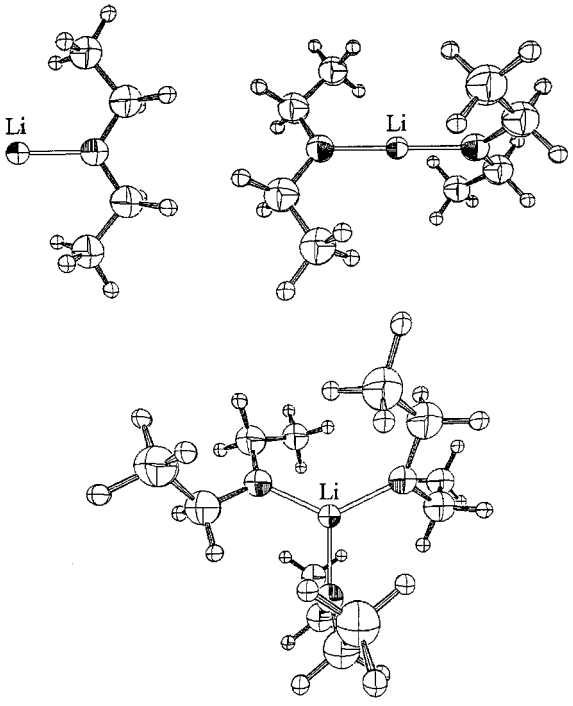

Figure 4. Calculated HF/6-311+G(d,p) structures for $Li^+\cdot(DEE)_{1-3}$. Oxygen atoms are partially shaded. The energetics and some geometrical parameters for all three structures are given in Table 1.

those calculated for $Li^+\cdot(DME)_{1-2}$ by More et al.[11] Unlike $Li^+\cdot(DME)_3$, the D_3-symmetric structure for $Li^+\cdot(DEE)_3$ shows some steric effects. The conformation of the carbon−oxygen backbones in $Li^+\cdot(DEE)_{1-2}$ are all trans, which leaves all of the heavy atoms of each Li−DEE moiety in one plane. On the other hand, those in $Li^+\cdot(DEE)_3$ are mixed with the trans and gauche forms; one DEE is all trans, and two DEEs have both a trans and gauche ethyl group. The $Li^+\cdot(DEE)_3$ complex with an all trans DEE conformation in D_3 symmetry lies 1.0 kcal mol^{-1} higher in energy than the structure shown in Figure 4, whereas that with all three DEEs having a trans−gauche conformation lies 0.5 kcal mol^{-1} higher in energy. In going from $n = 1$ to $n = 3$, the Li−O bond distance increases from 1.807 Å to an average 1.946 Å, in increments of 0.054 and 0.085 Å, while the C−O bond distance decreases from 1.430 Å to an average 1.424 Å by decrements of 0.004 and 0.002 Å. As the C−O bond decreases, the C−O−C bond angle decreases concomitantly. In free DEE, the C−O bond distance is 1.396 Å, and the C−O−C bond angle is 114.8°. A reduced C−O−C bond angle of 112.7° for the trans DEE in $Li^+\cdot(DEE)_3$, along with the significant increase in the Li−O bond distance and changes in ethyl conformation, suggests that steric hindrance is present. The calculated Li^+−DEE bond energies are 42.9, 32.5, and 13.6 kcal mol^{-1} for $n = 1-3$, respectively. The total solvation energy for $Li^+\cdot(DEE)_3$ is 89.0 kcal mol^{-1}.

Solvation versus Ligand Exchange. FT-ICR experiments afford a unique opportunity for studying the solvation mechanism in the gas phase. The $Li^+\cdot$(acetone-h_6)(acetone-d_6) complex was isolated in the ICR cell and then allowed to collide with a nearly 1:1 mixture of acetone-h_6 (H) and acetone-d_6 (D). According to Raoult's law, a nearly equivalent H/D mixture has nearly the same vapor pressure.[28] The solvation mechanism is outlined in eqs 4−7.

$$Li^+\cdot(HD) + L \xrightarrow{k_c} [Li^+\cdot(HDL)]^* \tag{4}$$

$$[Li^+\cdot(HDL)]^* \xrightarrow{k_{uni}} \begin{cases} Li^+\cdot(HD) + L \\ Li^+\cdot(LD) + H \\ Li^+\cdot(HL) + D \end{cases} \tag{5}$$

$$[Li^+\cdot(HDL)]^* \xrightarrow{1/\tau} Li^+\cdot(HDL) + h\nu \tag{6}$$

$$[Li^+\cdot(HDL)]^* + L \xrightarrow{k_q} Li^+\cdot(HDL) + L \tag{7}$$

Here, L can be either H or D, and $[Li^+\cdot(HDL)]^*$ is the bimolecular ion−molecule collision complex. The ion−molecule collision rate constant is k_c, k_{uni} is the unimolecular dissociation rate constant, $1/\tau$ is the radiative-cooling rate, and k_q is the bimolecular collisional quenching rate constant. In brief, $Li^+\cdot$(HD) collides with L to form $[Li^+\cdot(HDL)]^*$, which subsequently dissociates to $Li^+\cdot(HD)$, $Li^+\cdot(HH)$, or $Li^+\cdot(DD)$ via unimolecular dissociation, or it retains its stability via either radiative cooling or collisional quenching. Figure 5 shows a sample time plot at a total acetone pressure of 7.7×10^{-7} Torr. It clearly exhibits the relatively fast solvent-exchange process, restoring the 1:2:1 statistical distribution, which competes with the slower solvation. The pseudo-first-order rate constants for dissociative solvent-exchange and associative solvation are given by eqs 8 and 9.

$$k_{dissoc} = \frac{k_{uni}}{k_{uni} + 1/\tau + k_q[L]} k_c[L] \tag{8}$$

$$k_{assoc} = \frac{(1/\tau + k_q[L])}{k_{uni} + 1/\tau + k_q[L]} k_c[L] \tag{9}$$

These rate constants were measured as a function of the total

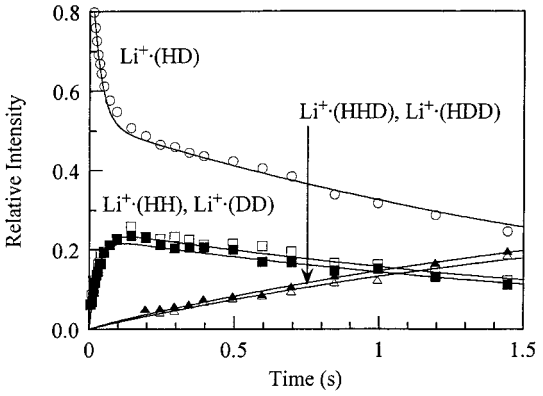

Figure 5. Time plot of the isolated Li^+·(HD) species (○) reacting with acetone-h_6 (H) and acetone-d_6 (D): Li^+·(HH) (□), Li^+·(DD) (■), Li^+·(HHD) (△), and Li^+·(HDD) (▲). Although not shown, Li^+·(HHH) and Li^+·(DDD) are observed in equal amounts after 0.5 s with approximately one-third the intensity of Li^+·(HHD) and Li^+·(HDD).

TABLE 2: Pseudo-first-Order Rates (s^{-1}) of Solvent-Exchange and Associative Solvation Reactions

pressure ($\times 10^{-7}$ Torr)	$Li^+(HD) + H$		$Li^+(HD) + D$	
	k_{dissoc}	k_{assoc}	k_{dissoc}	k_{assoc}
0.5	1.41	.008	1.14	.008
1.1	3.45	.023	2.88	.023
2.3	7.26	0.056	6.09	0.061
7.7	24.09	0.256	23.46	0.351
11.9	45.6	0.637	39.3	0.716

pressure of the 1:1 H/D mixture, and the results are summarized in Table 2. To simplify the data analysis, the two rate constants are added to give eq 10, and the ratio of k_{assoc} to k_{dissoc} is taken to yield eq 11.

$$k_{assoc} + k_{dissoc} = k_c\,[L] \tag{10}$$

$$\frac{k_{assoc}}{k_{dissoc}} = \frac{1/\tau + k_q[L]}{k_{uni}} \tag{11}$$

Figure 6(a) shows the pressure dependence of $k_{assoc} + k_{dissoc}$. A least-squares fit to the four low-pressure data points, yields $k_c = 1.95 \times 10^{-9}$ and 1.88×10^{-9} cm^3 molecule^{-1} s^{-1} for Li^+·(HD) + H and Li^+·(HD) + D reactions, respectively. Absolute errors are estimated to be ±25%, due to uncertainties in absolute pressure measurements. The relative errors should be much less. The ratio $k_{c,Li^+\cdot(HD)+D}/k_{c,Li^+\cdot(HD)+H} = 0.963$ is in excellent agreement with a value of 0.967, estimated from the Langevin model of the ion−molecule collision rate constant, eq 12.

$$\frac{k_{c,Li^+\cdot(HD)+D}}{k_{c,Li^+\cdot(HD)+H}} = \sqrt{\frac{\mu_{Li^+\cdot(HD)+H}}{\mu_{Li^+\cdot(HD)+D}}} \tag{12}$$

where μ is the reduced mass. A least-squares fit to the plot of the ratio k_{assoc}/k_{dissoc} as a function of [L], as shown in Figure 6b, results in $1/\tau k_{uni}$ from the intercept and k_q/k_{uni} from the slope. To estimate $1/\tau$ and k_{uni}, we assume that the collisional-quenching rates are limited by the ion−molecule collision frequency. The Langevin model suggests that $k_{c,Li^+\cdot(HHD)+H} = 0.950k_{c,Li^+\cdot(HD)+H}$ and $k_{c,Li^+\cdot(HHD)+D} = 0.947k_{c,Li^+\cdot(HD)+D}$ and that $k_{c,Li^+\cdot(HDD)+H} = 0.947k_{c,Li^+\cdot(HD)+H}$ and $k_{c,Li^+\cdot(HDD)+D} = 0.943k_{c,Li^+\cdot(HD)+D}$. Thus, the collisional quenching rate constants are estimated to be $k_q \le 1.82 \times 10^{-9}$ cm^3 molecule^{-1} s^{-1} for [Li^+·(HHD)]* + L and $k_q \le 1.81 \times 10^{-9}$ cm^3 molecule^{-1} s^{-1} for [Li^+·(HDD)]* + L. These limiting values for k_q lead to $k_{uni} \le$ 8700 ± 2200 s^{-1} and $1/\tau \le 49 \pm 12$ s^{-1} for [Li^+·(HHD)]* and $k_{uni} \le 6100 \pm 1500$ s^{-1} and $1/\tau \le 43 \pm 11$ s^{-1} for [Li^+·(HDD)]*, from a linear fit to the data shown in Figure 6b. Errors are due to uncertainties in the absolute pressure measurements. Therefore, the lifetimes of ion−molecule collision complexes are derived from k_{uni}'s; ∼110 μs for [Li^+·(HHD)]* and ∼160 μs for [Li^+·(HDD)]*. It appears that the acetone-d_6 substitution affords the collision complex more longevity. In the $0.5-11.9 \times 10^{-7}$ Torr pressure range used in this work, the collisional quenching rates are on the order of 3−70 s^{-1}. Thus, both the collisional quenching and the radiative cooling are responsible for associative solvation in this pressure range. The present result also confirms that in a low-pressure range (<10^{-8} Torr) the ion−molecule association will take place predominantly via radiative cooling, whereas in the high-pressure range (above 10^{-5} Torr), the association will occur mostly via collisional quenching.[7]

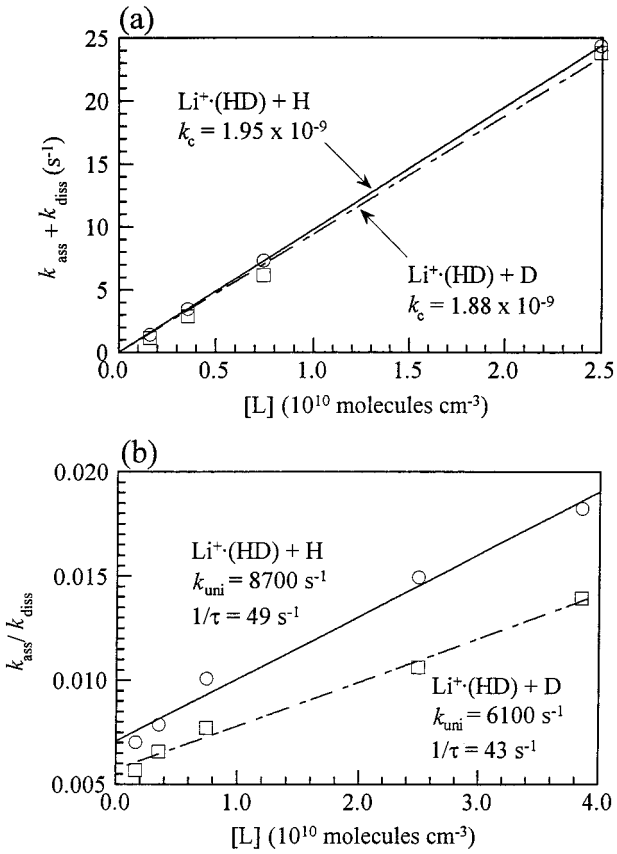

Figure 6. (a) $k_{assoc} + k_{dissoc}$ as a function of pressure: Li^+·(HD) + H (○) and Li^+·(HD) + D (□). The slope represents the bimolecular ion−molecule collision rate constant, k_c. (b) k_{assoc}/k_{dissoc} as a function of pressure: Li^+·(HD) + H (○) and Li^+·(HD) + D (□). The slope is k_q/k_{uni} and the intercept is $1/\tau k_{uni}$.

Phase Space Calculations. To directly estimate the k_{uni} of the collision complex, the PST[21−23] was employed. Scaled Hartree−Fock vibrational frequencies obtained at RHF/6-31G* level were used with the Beyer−Swinehart direct state-count method to determine the density of states and the sum of states.[29] The hindered internal methyl rotation in acetone, with a barrier height of $V_{eff} = 291$ cm^{-1}, is treated as a free rotor with the rotational constant $B = 17.0$ and 8.5 cm^{-1} for acetone-h_6 and acetone-d_6, respectively. Additionally, there is a near-free internal rotation of acetone in Li^+·(acetone)$_2$, with $B = 2.0$, 1.76, and 1.56 cm^{-1} for Li^+·(HH), Li^+·(HD), and Li^+·(DD), respectively. For Li^+·(acetone)$_3$, there is an additional hindered rotation of acetone with a barrier height of $V_{HF} = 189$ cm^{-1}.

TABLE 3: Parameters Used for the PST Calculations

parameter	value	parameter	value[a] (eV)
α(acetone)	6.33 Å^3	D_0 ($HHLi^+-H$)	1.0815
B(H)	0.2530 cm^{-1}	D_0 ($HHLi^+-D$)	1.0832
B(D)	0.2026 cm^{-1}	D_0 ($HDLi^+-H$)	1.0819
B(Li^+·HH)	0.0294 cm^{-1}	D_0 ($HDLi^+-D$)	1.0837
B(Li^+·HD)	0.0265 cm^{-1}	D_0 ($DDLi^+-H$)	1.0815
B(Li^+·DD)	0.0241 cm^{-1}	D_0 ($DDLi^+-D$)	1.0832
B(Li^+·HHH)	0.0128 cm^{-1}		
B(Li^+·HHD)	0.0114 cm^{-1}		
B(Li^+·HDD)	0.0121 cm^{-1}		
B(Li^+·DDD)	0.0108 cm^{-1}		

[a] Dissociation energies were calculated at the HF level with a 6-31G* basis set for C, O, H and a 6-311G* basis set for Li.

These three degenerate rotational constants are estimated at B = 1.0 and 0.79 cm^{-1} for internal rotation of acetone-h_6 and acetone-d_6, respectively. The rotational constants of all of the molecular species were approximated to their spherical values, that is, $B = 3\sqrt{B_xB_yB_z}$. Molecular parameters used in the PST calculations are listed in Table 3. Also included in Table 3 are the theoretical dissociation thresholds obtained at the RHF level with a 6-31G* basis set for C, O, and H and a 6-311G* basis set for Li. This level of theory predicts the Li−acetone bond dissociation energy for Li^+·(acetone)$_3$ in excellent agreement with experiment, which is fortuitous because of the cancellation of errors. Vibrational frequencies, including the internal rotations, are listed in Table 4. The resulting rate-energy curves for the loss of a specific acetone (i.e., the reaction degeneracy σ = 1) are shown in Figure 7. The unimolecular dissociation rate constant, k_{PST}, decreases with increasing acetone-d_6 substitution as follows: k_{PST}[Li^+·(HHH)] > k_{PST}[Li^+·(HHD)] > k_{PST}[Li^+·(HDD)] > k_{PST}[Li^+·(DDD)]. For mixed clusters Li^+·(HHD) and Li^+·(HDD), the difference in rate between the loss of acetone-h_6 and acetone-d_6 is not discernible in Figure 7. The unimolecular dissociation rate is obtained at the average internal energy of the collision complex formed by thermal collisions of Li^+·(acetone)$_2$ with acetone at 298 K. The results are summarized in Table 5. Taking into account the thermal energies of the collision partners results in the excess internal energy of 0.325, 0.340, 0.355, and 0.368 eV above the dissociation threshold for [Li^+·(HHH)]*, [Li^+·(HHD)]*, [Li^+·(HDD)]*, and [Li^+·(DDD)]*, respectively. On average, [Li^+·(HHH)]* dissociates to Li^+·(HH) + H with the rate k_{PST} = 12 300 s^{-1}, [Li^+·(HHD)]* dissociates to either Li^+·(HH) + D or Li^+·(HD) + H with k_{PST} = 8030 s^{-1}, [Li^+·(HDD)]* dissociates to either Li^+·(HD) + D or Li^+·(DD) + H with k_{PST} = 5440 s^{-1}, and [Li^+·(DDD)]* dissociates to Li^+·(DD) + D with k_{PST} = 3540 s^{-1}. The theoretical values of k_{PST} = 8030 and 5440 s^{-1} for [Li^+·(HHD)]* and [Li^+·(HDD)]*, respectively, are in excellent agreement with experimental values of $k_{uni} \leq 8700 \pm 2200$ and 6100 ± 1500 s^{-1}, respectively.

Discussion

The absolute BDEs determined from our experiments are compared with the theoretical results obtained at the HF/6-311+G(d,p) level in Table 6 and shown graphically in Figure 8. Also included in Table 6 are the values for the bond dissociation enthalpies of Li^+·(S) that are derived from the ICR bracketing equilibrium measurements by Taft et al.,[9] which are calibrated against $D_{298}(Li^+-OH_2)$ = 32.7 kcal mol^{-1} as recommended by Rodgers and Armentrout.[10] In the case of Li^+·(S), our theoretical results are 2−5 kcal mol^{-1} higher than our experimental results, likely indicating an overestimation of the Li−O interactions at the HF level, as the basis set superposition error estimated by the counterpoise correction is less than 1 kcal mol^{-1}. This electron-correlation error, inherent in the HF calculations, diminishes with increasing solvation number, presumably because of the cancellation of errors from basis-set deficiency with electron-correlation deficiency. In the case of Li^+·(S)$_3$, theoretical binding energies are 1−2 kcal mol^{-1} lower than the experimental binding energies, indicating the electron-correlation deficiency. The slope in Figure 8 suggests that the solvent binding energies decrease by 9−12 kcal mol^{-1} per increase in the solvation number, with the exception of the third DEE solvation, which is lowered by 19 kcal mol^{-1}.

Theoretical structures and energetics suggest that the maximum solvation number in the first solvation shell is four for acetone and THF and three for DEE. Although theory predicted D_{298}[(S)$_3$·Li^+-S] = 12.3 and 13.7 kcal mol^{-1} and $\Delta G_{298} = -2.5$ and −0.1 kcal mol^{-1} for the fourth coordination of acetone and THF, respectively, the Li^+·(S)$_4$ species were not observed at room temperature in the ICR cell. On the other hand, the Li^+·(DEE)$_3$ species with D_{298}[(S)$_2$·Li^+-S] = 13.4 kcal mol^{-1} and ΔG_{298} = −2.3 kcal mol^{-1} was readily observed at room temperature. The absence of the Li^+·(S)$_4$ species for acetone and THF in our experiments indicates a dynamic bottleneck in their gas-phase formation. The preexisting ligands in the Li^+·(S)$_3$ species, in D_3 symmetry for acetone and THF, dynamically hinder the formation of the n = 4 coordination complexes in tetrahedral geometry. In the case of DEE, the third DEE binding energy of 15 kcal mol^{-1} is ∼9 kcal mol^{-1} less than those for acetone and THF. This significant difference is ascribed to steric repulsion among the ethyl groups in the Li^+·(DEE)$_3$ structure, causing the ethyl groups in two DEEs to rotate internally to have both trans and gauche conformations. In condensed phase, there are reports of solvated complexes of lithium halides by THF and DEE, such as [LiCl·2THF]$_2$,[30,31] [LiCl·THF]$_\infty$,[32] and pseudotetrahedral [LiBr·DEE]$_4$,[33] whereas no lithium halide complexes solvated by acetone have been reported to date.

The lifetime of the [Li^+·(acetone)$_3$]* complex can be compared with that of the protonated acetone dimer, [H^+·(acetone)$_2$]*, reported by McMahon and co-workers.[34,35] In their experiment, the kinetics of low-pressure association reactions of protonated acetone with acetone was measured by using FT-ICR spectrometry. The ion−molecule collision rate constant was determined from trajectory calculations and the unimolecular dissociation rate and the radiative cooling rate were derived from the plot of the apparent association rate constant as a function of pressure. The lifetimes of proton-bound dimers were 41 μs for H^+·(acetone-h_6)$_2$ at 300 K and 112 μs for H^+·(acetone-d_6)$_2$ at 297 K, while the estimated lifetimes of [Li^+·(acetone)$_3$]* were ∼110 μs for [Li^+·(HHD)]* and ∼160 μs for [Li^+·(HDD)]* at 298 K. The pronounced longevity for [Li^+·(acetone)$_3$]* is due to the increase in the internal degrees of freedom in tricoordination of acetone (87 for [Li^+·(acetone)$_3$]* vs 57 for [H^+·(acetone)$_2$]*). The isotope effect on k_{uni} is also apparent in Table 5. PST predicts the decrease of k_{uni} with increasing acetone-d_6 substitution: k_{uni} = 12300, 8030, 5440, and 3540 s^{-1} for [Li^+·(HHH)]*, [Li^+·(HHD)]*, [Li^+·(HDD)]*, and [Li^+·(DDD)]*, respectively. In protonated acetone, the reported k_{uni} values are 49 000, 47 000, 16 900, and 14 900 s^{-1} for [D^+·(acetone-h_6)$_2$]*, [H^+·(acetone-h_6)$_2$]*, [D^+·(acetone-d_6)$_2$]*, and [H^+·(acetone-d_6)$_2$]*, respectively, at 320 K.[34] k_{uni} decreases with increasing acetone-d_6 substitution where the loss of acetone-h_6 occurs faster than that of acetone-d_6. This same trend is observed here with [Li^+·(HHD)]* and [Li^+·(HDD)]* complexes.

The radiative cooling rate for the Li^+·(acetone)$_3$ system shows an isotope effect; $1/\tau = 49 \pm 12$ s^{-1} for [Li^+·(H_2D)]*, compared

TABLE 4: Vibrational Frequencies Used for the Phase Space Theory Calculations

molecule	frequencies (cm^{-1})[a]
acetone-h_6	(17, 17) 366, 485, 525, 773, 895, 898, 188, 1132, 1235, 1412, 1420, 1468, 1471, 1474, 1491, 1847, 2927, 2934, 2977, 2985, 3035, 3036
acetone-d_6	(8.5, 8.5) 308, 404, 474, 680, 684, 720, 895, 991, 1027, 1057, 1063, 1063, 1074, 1118, 1265, 1840, 2107, 2111, 2203, 2210, 2250, 2253
Li^+·(HH)	(2.0, 17, 17, 17, 17) 19, 19, 58, 59, 153, 157, 158, 366, 392, 489, 489, 521, 521, 640, 792, 810, 890, 890, 921, 921, 1096, 1099, 1132, 1133, 1264, 1264, 1418, 1418, 1425, 1425, 1455, 1455, 1459, 1459, 1469, 1469, 1483, 1483, 1759, 1775, 2932, 2932, 2937, 2937, 2994, 2994, 2999, 2999, 3043, 3043, 3044, 3044
Li^+·(HD)	(1.76, 8.5, 8.5, 17, 17) 18, 18, 53, 57, 148, 155, 157, 320, 381, 407, 472, 489, 521, 627, 672, 719, 739, 801, 890, 915, 921, 995, 1034, 1049, 1052, 1055, 1067, 1098, 1127, 1132, 1264, 1288, 1418, 1425, 1455, 1459, 1469, 1483, 1753, 1771, 2110, 2115, 2214, 2219, 2258, 2261, 2932, 2937, 2994, 2999, 3043, 3044
Li^+·(DD)	(1.56, 8.5, 8.5, 8.5, 8.5) 17, 17, 52, 53, 143, 155, 155, 310, 335, 407, 407, 472, 472, 617, 668, 674, 709, 729, 737, 737, 909, 921, 994, 995, 1034, 1034, 1049, 1049, 1052, 1052, 1055, 1055, 1067, 1067, 1127, 1127, 1288, 1288, 1749, 1765, 2110, 2110, 2115, 2115, 2214, 2214, 2219, 2219, 2258, 2258, 2261, 2261
Li^+·(HHH)	(1.0, 1.0, 1.0, 17, 17, 17, 17, 17, 17) 12, 13, 13, 20, 20, 22, 26, 26, 64, 133, 133, 137, 181, 361, 361, 386, 489, 489, 489, 506, 506, 520, 520, 522, 790, 794, 794, 892, 892, 892, 915, 915, 915, 1096, 1096, 1096, 1133, 1134, 1134, 1258, 1258, 1259, 1418, 1418, 1419, 1426, 1426, 1426, 1460, 1460, 1460, 1461, 1461, 1461, 1470, 1470, 1470, 1484, 1485, 1485, 1785, 1785, 1809, 2932, 2932, 2932, 2939, 2939, 2939, 2990, 2990, 2990, 2997, 2997, 2997, 3040, 3040, 3040, 3041, 3041, 3041
Li^+·(HHD)	(0.79, 1.0, 1.0, 8.5, 8.5, 17, 17, 17, 17) 20, 20, 22, 24, 26, 60, 129, 132, 135, 181, 313, 361, 379, 408, 471, 488, 489, 501, 506, 520, 521, 674, 706, 732, 791, 794, 892, 892, 909, 915, 915, 995, 1034, 1053, 1053, 1057, 1069, 1096, 1096, 1125, 1134, 1134, 1258, 1259, 1283, 1418, 1419, 1426, 1426, 1460, 1460, 1461, 1461, 1470, 1470, 1485, 1485, 1778, 1785, 1807, 2110, 2115, 2212, 2218, 2255, 2258, 2932, 2932, 2939, 2939, 2990, 2990, 2997, 2997, 3040, 3040, 3041, 3041
Li^+·(HDD)	(0.79, 0.79, 1.0, 8.5, 8.5, 8.5, 8.5, 17, 17) 19, 19, 21, 24, 25, 57, 124, 131, 131, 180, 308, 320, 371, 408, 408, 470, 472, 487, 497, 502, 521, 673, 674, 705, 707, 732, 732, 793, 892, 908, 910, 915, 995, 996, 1033, 1034, 1053, 1053, 1053, 1053, 1057, 1057, 1068, 1069, 1096, 1125, 1125, 1134, 1258, 1283, 1284, 1418, 1426, 1460, 1461, 1470, 1485, 1776, 1781, 1804, 2110, 2110, 2115, 2115, 2212, 2212, 2218, 2218, 2255, 2255, 2258, 2258, 2932, 2939, 2990, 2997, 3040, 3041
Li^+·(DDD)	(0.79, 0.79, 0.79, 8.5, 8.5, 8.5, 8.5, 8.5, 8.5) 19, 19, 20, 23, 23, 55, 124, 124, 128, 180, 308, 308, 329, 407, 408, 408, 470, 470, 472, 494, 494, 673, 674, 674, 704, 707, 707, 732, 732, 732, 907, 910, 910, 995, 996, 996, 1033, 1033, 1034, 1053, 1053, 1053, 1053, 1053, 1053, 1057, 1057, 1057, 1068, 1069, 1069, 1125, 1125, 1126, 1283, 1283, 1284, 1776, 1776, 1800, 2110, 2110, 2110, 2115, 2115, 2115, 2212, 2212, 2212, 2218, 2218, 2218, 2255, 2255, 2255, 2258, 2258, 2258

[a] Values in parentheses are the internal rotational constants replacing a vibration.

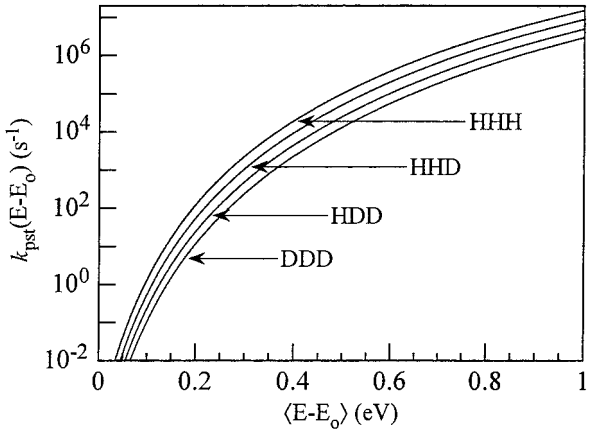

Figure 7. Rate/energy curves from PST calculations for the unimolecular dissociation of Li^+·(acetone)$_3$. Curves are labeled with H and D representing acetone-h_6 and acetone-d_6, respectively. For the mixed complexes the channels for H or D loss are indistinguishable on this scale.

TABLE 5: Average Thermal Dissociation Rates for [Li^+·(acetone)$_3$]* at 298 K

dissociation channel	σ[a]	$\langle E - E_0 \rangle_{298K}$[b]	k_{PST} (10^3 s^{-1})
Li^+·(HH) + H	3	0.325	12.3
Li^+·(HH) + D	1	0.340	2.60
Li^+·(HD) + H	2	0.340	5.43
Li^+·(HD) + D	2	0.355	3.55
Li^+·(DD) + H	1	0.355	1.89
Li^+·(DD) + D	3	0.368	3.54

[a] The reaction degeneracy; this factor is included in the rate constant. [b] Average internal energy in eV of the collision complex above the dissociation threshold E_0.

to $1/\tau = 43 \pm 11$ s^{-1} for [Li^+·(HD_2)]*. According to Dunbar,[36] provided that the transition dipole moments are the same, the frequency that contributes most to the radiative cooling rate is $\nu_{max} = 2kT/h$, where T is the internal temperature of the collision complex. When the ion−molecule collision complex is formed under a single-collision condition, the internal energy available in the complex is the sum of the solvation enthalpy and thermal energy of the reactants. The internal temperature of the collision complex is estimated by taking into account the thermal energy of the reactants at 298 K listed in Table 5 as $\langle E - E_0 \rangle_{298K}$ and the third-acetone solvation energy listed in Table 3. The internal energy of the collision complexes are estimated to be 1.407, 1.423, 1.438, and 1.451 eV above the zero-point energy level for [Li^+·(HHH)]*, [Li^+·(HHD)]*, [Li^+·(HDD)]*, and [Li^+·(DDD)]*, respectively, and the corresponding internal temperatures are 523, 547, 537 and 528 K, respectively. Therefore, the IR frequency contributing most to the radiative cooling rate is 727, 760, 746, and 734 cm^{-1} for [Li^+·(HHH)]*, [Li^+·(HHD)]*, [Li^+·(HDD)]*, and [Li^+·(DDD)]*, respectively. Because the radiative rate is proportional to ν^3, this simple model predicts that higher internal temperatures yield faster radiative cooling rates. The faster radiative cooling rate observed for [Li^+·(HHD)]* compared to [Li^+·(HDD)]* may be due to the higher internal temperature of the collision complex.

TABLE 6: Bond Dissociation Enthalpy and Free Energy of the Li^+·$(S)_n$ Product at 298 K in Kcal Mol^{-1}

	$D_{298}[Li^+\cdot(S)_{n-1}-S]$		
species	expt[a]	theory[b]	$-\Delta G_{298}$(theory)[c]
Li^+·(acetone)	44[d]	48.6	39.2
Li^+·(acetone)$_2$		37.1	30.6
Li^+·(acetone)$_3$	24.4 (0.6)	22.4	14.9
Li^+·(acetone)$_4$		12.3	2.5
Li^+·(THF)	40[d]	44.1	37.9
Li^+·(THF)$_2$		35.3	27.6
Li^+·(THF)$_3$	24.1 (0.6)	23.0	13.1
Li^+·(THF)$_4$		13.7	0.1
Li^+·(DEE)	41[d]	43.3	36.9
Li^+·(DEE)$_2$		32.0	22.4
Li^+·(DEE)$_3$	15.0 (0.4)	13.4	2.3

[a] This work, except where noted; the 95% confidence interval is given in parentheses. [b] HF/6-311+G(d,p) optimized energies, with zero-point energy corrections determined by RHF vibrational frequencies scaled by 0.9135. [c] HF/6-311+G(d,p) enthalpies and entropies calculated from the scaled RHF vibrational frequencies and rational constants by using statistical mechanics. [d] Values from Taft et al. (ref 9) are converted to the 298 K values and calibrated against a value of $D_{298}(Li^+-OH_2) = 32.7$ kcal mol^{-1} (ref 10).

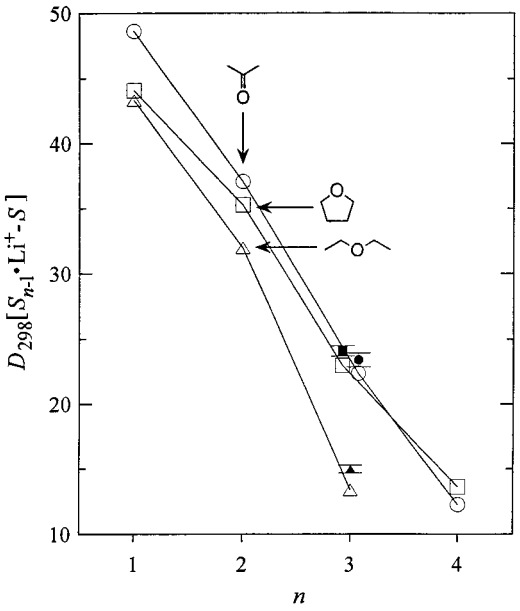

Figure 8. Comparison of the theoretical $(S)_{n-1}\cdot Li^+-S$ bond enthalpies (open symbols) with the experimental enthalpies (filled symbols) examined in this work; units are in kcal mol^{-1}. Acetone and THF points are offset at $n = 3$ for clarity.

Conclusion

FT-ICR solvation equilibrium measurements have yielded absolute solvent-binding energies that can be used as reference values for other experiments and theory. In light of theoretical structures, and experimental and theoretical solvation energies, steric factors involved in the formation of solvated complexes were elucidated. Although thermodynamically allowed, the dynamic bottleneck involved in the fourth coordination of acetone and THF hinders the formation of the $Li^+\cdot(S)_4$ species in the gas phase at room temperature. The bulky ethyl groups in diethyl ether result in significant steric repulsion of the third coordination of diethyl ether to $Li^+\cdot(DEE)_2$. The kinetics of solvent exchange and association processes provide a detailed understanding of the association reaction mechanism, the isotope effect in the unimolecular dissociation rate and the radiative cooling rate of the collision complex. The unimolecular dissociation rate decreases with increasing acetone-d_6 substitution, and the loss of acetone-h_6 occurs faster than that of acetone-d_6. The radiative cooling rate depends on the extent of internal excitation in the collision complex formed from bimolecular ion−molecule collisions.

Acknowledgment. S.K.S. acknowledges the support from the National Science Foundation Young Investigator Award CHE-9457668, the Arnold Mabel Beckman Foundation Young Investigator Award, and the Pohang University of Science and Technology.

References and Notes

(1) *Lithium Chemistry: A Theoretical and Experimental Overview*; Sapse, A.-M., Schleyer, P. v. R., Ed; Wiley: New York, 1995.
(2) Loupy, A.; Tchoubar, B. *Salt Effects in Organic and Organometallic Chemistry*; VCH: Weinheim, 1992.
(3) Friedman, H. L. *Annu. Rev. Phys. Chem.* **1981**, *32*, 179.
(4) Dzidic, I.; Kebarle, P. *J. Phys. Chem.* **1970**, *74*, 1466.
(5) Wieting, R. D.; Staley, R. H.; Beauchamp, J. L. *J. Am. Chem. Soc.* **1975**, *97*, 924.
(6) Staley, R. H.; Beauchamp, J. L. *J. Am. Chem. Soc.* **1975**, *97*, 5920.
(7) Woodin, R. L.; Beauchamp, J. L. *J. Am. Chem. Soc.* **1978**, *100*, 501.
(8) Woodin, R. L.; Beauchamp, J. L. *Chem. Phys.* **1979**, *41*, 1.
(9) Taft, R. W.; Anvia, F.; Gal, J.-F.; Walsh, S.; Capon, M.; Holmes, M. C.; Hosn, K.; Oloumi, G.; Vasanwala, R.; Yazdani, S. *Pure Appl. Chem.* **1990**, *62*, 17.
(10) Rodgers, M. T.; Armentrout, P. B. *J. Phys. Chem. A* **1997**, *101*, 1238.
(11) More, M. B.; Glendening, E. D.; Ray, D.; Feller, D.; Armentrout, P. B. *J. Phys. Chem.* **1996**, *100*, 1605.
(12) Ray, D.; Feller, D.; More, M. B.; Glendening, E. D.; Armentrout, P. B. *J. Phys. Chem.* **1996**, *100*, 16116.
(13) Rodgers, M. T.; Armentrout, P. B. *J. Phys. Chem. A* **1997**, *101*, 2614.
(14) Rodgers, M. T.; Armentrout, P. B. *J. Chem. Phys.* **1998**, *109*, 1787.
(15) Jarek, R. L.; Shin, S. K. *J. Am. Chem. Soc.* **1997**, *119*, 10501.
(16) Jarek, R. L.; Denson, S. C.; Shin, S. K. *J. Chem. Phys.* **1998**, *109*, 4258.
(17) Ollmann, B.; Kupka, K. D.; Hillenkamp, F. *Int. J. Mass Spectrom. Ion Processes* **1983**, *47*, 31.
(18) Karas, M.; Bachmann, D.; Bahr, U.; Hillenkamp, F. *Int. J. Mass Spectrom. Ion Processes* **1987**, *78*, 53.
(19) Karas, M.; Bahr, U.; Hillenkamp, F. *Int. J. Mass Spectrom. Ion Process* **1989**, *92*, 231.
(20) Rodgers, M. T.; Ervin, K. M.; Armentrout, P. B. *J. Chem. Phys.* **1997**, *106*, 4499.
(21) Chesnavich, W. J.; Bowers, M. T. *J. Chem. Phys.* **1977**, *66*, 2306.
(22) Chesnavich, W. J.; Bowers, M. T. *J. Am. Chem. Soc.* **1977**, *99*, 1705.
(23) Chesnavich, W. J.; Bowers, M. T. In *Gas-Phase Ion Chemistry, Vol. 1*; Bowers, M. T., Ed.; Academic Press: New York, 1979; pp 119−151.
(24) Shin, S. K.; Han, S.-J.; Kim, B. J. *J. Am. Soc. Mass Spectrom.* **1996**, *7*, 1018.
(25) Frisch, M. J. et al. *Gaussain 94, Revision C.2.*; Gaussian, Inc.: Pittsburgh, PA, 1995.
(26) (a) McLean, A. D.; Chandler, G. S. *J. Chem. Phys.* **1980**, *72*, 5639. (b) Krishnan, R.; Binkley, J. S.; Seeger, R.; Pople, J. A. *J. Chem. Phys.* **1980**, *72*, 650.
(27) Scott, A. P.; Radom, L. *J. Phys. Chem.* **1996**, *100*, 16502.
(28) Electron impact mass spectra of the sample containing both acetone-h_6 (bp 56.1 °C) and acetone-d_6 (bp 55.5 °C) confirm the same parent ion intensities to within 2%.
(29) Beyer, T.; Swinehart, D. R. *ACM Commun.* **1973**, *16*, 379.
(30) Hahn, F. E.; Rupprecht, S. *Z. Naturforsch.* **1991**, *46b*, 143.
(31) De Angelis, S.; Solari, E.; Gallo, E.; Floriani, C.; Chiesi-Villa, A.; Rizzdi, C. *Inorg. Chem.* **1991**, *30*, 3978.
(32) Edwards, A. J.; Paver, M. A.; Raithby, P. R.; Russel, C. A.; Wright, D. S. *J. Chem. Soc., Dalton Trans.* **1993**, 3265.
(33) Neumann, F.; Hampel, F.; Schleyer, P. v. R. *Inorg. Chem.* **1995**, *34*, 6553.
(34) Kofel, P.; McMahon, T. B. *J. Phys. Chem.* **1988**, *92*, 6174.
(35) Thölmann, D.; McCormick, A.; McMahon, T. B. *J. Phys. Chem.* **1994**, *98*, 1156.
(36) Dunbar, R. C. *Int. J. Mass Spectrom. Ion Processes* **1990**, *100*, 423.